Composite Structures 184 (2018) 1062–1070

Contents lists available at ScienceDirect

Composite Structures

journal homepage: www.elsevier.com/locate/compstruct

Stability considerations and actuation requirements in bistable laminated composites

V.S.C. Chillara, M.J. Dapino*

NSF IUCRC on Smart Vehicle Concepts, Department of Mechanical and Aerospace Engineering, The Ohio State University, Columbus, OH 43210, USA

ARTICLE INFO

Keywords:
Bistable
Morphing
High-order model
Actuation
Fiber-reinforced elastomer

ABSTRACT

Laminated composites with a core layer sandwiched between orthogonal mechanically-prestrained laminae exhibit two weakly-coupled cylindrical shapes where each shape is influenced only by one prestrained lamina. This study investigates the domain of bistability and actuation requirements of such bistable laminated composites. An analytical model is constructed as follows: point-wise displacements and areal dimensions are scaled; strain energy and actuation work are computed using high-order displacement polynomials; and net energy is minimized using the Rayleigh-Ritz method to calculate stable shapes as a function of actuation force. Shape transition is shown to be a multi-stage phenomenon through an experimental procedure involving friction-free tensile tests and 3D motion capture. The simulated actuation energies agree with measurements within 12%. Square laminates are shown to be bistable only when the ratios of laminae prestrains are greater than 0.2. The aspect ratio limit for bistability can be improved by maximizing both prestrains while maintaining a prestrain ratio of one. It is shown that in-plane forcing requires 100 times more energy than an equivalent moment. A parametric study reveals that the composite's performance parameters are more sensitive to the core's thickness than its modulus; the sensitivity of actuation energy is minimal relative to that of deformation and stiffness.

1. Background

1.1. Bistable composites

Advanced aircraft [1,2] and automobiles [3] require lightweight structural panels that change shape to optimize performance over a broad range of operating conditions. These panels often require adaptive elements that change their curvature in order to achieve global shape change. Bistable laminated composites are candidates for curved elements due to their ability to hold large deformed shapes in the absence of actuation forces; they require actuation only to hold an intermediate shape or to switch from one stable shape to another.

Curvature in a composite can be achieved by imparting residual stress; the approach is attractive because residual stress is an intrinsic feature. The most commonly studied bistable composites are thermally-cured fiber-reinforced polymeric (FRP) laminates. These laminates contain residual stress at room temperature due to a mismatch between the thermal contraction of the matrix and the fiber. Asymmetric FRP laminates may have multiple stable shapes that depend on fiber orientation, laminate size, and curing temperature [4]. In the case of symmetric laminates, bistability can be achieved by applying mechanical prestress to the fibers prior to thermal curing [5,6]. Li et al. [7] and Daynes et al. [8] presented hybrid FRP composites with sandwiched metal cores as a solution to augment curvature and improve robustness to operating conditions. The individual tailoring of the stable shapes of thermally-cured FRP laminates is limited by a globally applied residual stress that creates a strong coupling between the shapes.

Chillara et al. [9] demonstrated curved composites in which residual stress is imbued through mechanical prestrain in select laminae; this approach enables the stress-free laminae to bear adaptive features. Laminating two mechanically-prestressed layers on either side of a stress-free core results in a bistable composite [10]. When the prestressed laminae are orthogonal to each other, the equilibrium cylindrical shapes are said to be weakly coupled; each shape is influenced only by one prestressed lamina but not both. Residual stress generated through two sources of mechanical prestrain yields a domain of bistability that is different from that resulting from a single source (e.g., temperature in thermally-cured laminates). Therefore, a study exploring the limits of design parameters, such as prestrain ratio and aspect ratio, is required to determine the composite's bistability regime.

A bistable composite with orthogonal prestressed laminae exhibits three equilibrium shapes, of which two are stable. Therefore, the strain energy of the composite has two minima and one maximum. Switching between stable shapes, also known as snap-through, is achieved by

* Corresponding author.
E-mail addresses: chillara.1@osu.edu (V.S.C. Chillara), dapino.1@osu.edu (M.J. Dapino).

http://dx.doi.org/10.1016/j.compstruct.2017.09.097
Received 4 June 2017; Received in revised form 20 August 2017; Accepted 28 September 2017
Available online 10 October 2017
0263-8223/

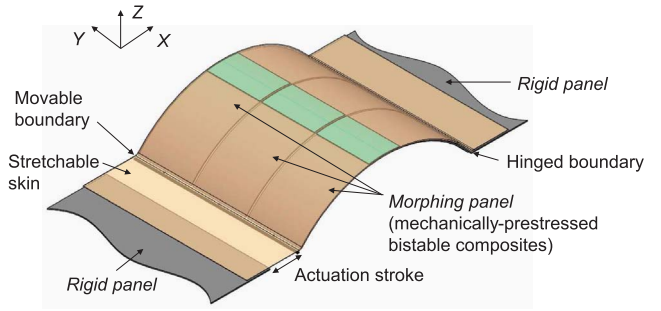

Fig. 1. Concept for a morphing structure configured with mechanically-prestressed bistable composites.

applying a force that is sufficient to overcome the strain energy maxima. The mode of actuation of a composite element depends on its boundary conditions within the host structure. Fig. 1 shows an example of a morphing structure that comprises an array of mechanically-prestressed composite ribs. One approach to actuation is to move the boundaries apart in the axial (*X*) direction so as to flatten the composites. A relevant example is the use of pneumatic muscles as linear actuators in the underlying structure of a spanwise-morphing aircraft wing [11]. Another actuation approach involves harnessing transverse (*Z*) operational loads acting on the composite. For example, a bistable wind turbine blade snaps into its second shape at a limiting value of gust load (normal pressure) to enable load alleviation [12].

In-plane actuation has been the preferred choice for bistable composites due to compactness and practical viability; smart materials such as piezoelectrics and shape memory alloys can be configured as active laminae. Piezoceramic (macro-fiber composite) laminae can contract when electrically-activated to recover the in-plane strain for actuation [13,14]. However, the low actuation strain (0.1 %) of piezoelectric actuators limits their application to composites with small curvature. Shape memory alloys (SMA) have a maximum strain of up to 6 % and can serve as embedded actuators for composites with large curvature [15–17]. Installing SMA wires on both faces of the composite yields a push-pull system where the actuation of each wire enables strain recovery in the antagonistic wire [18]. Fluid channels embedded in a flexible lamina can be pressurized to snap the composite into its second shape [19,20].

Despite the availability of a wide variety of actuator designs, the relative performance of various actuation modes such as axial, transverse, and in-plane loading is not well understood. Also, actuation energy is one performance metric for a bistable composite among others such as out-of-plane deformation (unactuated) and stiffness. Therefore, a sensitivity study of the composite's performance metrics is needed to guide material selection and geometric design.

1.2. Modeling of composite actuation

The equilibrium shapes of an asymmetric bistable composite were first modeled analytically by Hyer [21] using strain energy minimization. The composite was modeled as a laminated plate based on a Lagrangian strain formulation and classical laminate theory. Energy minimization was carried out using the Rayleigh-Ritz method and the resulting nonlinear equations were solved for the displacements of the composite. The energy-based analytical approach was further developed by Hamamoto and Hyer [22], and Dano and Hyer [23,24]. Schlecht and Schulte [25] presented a comprehensive finite element study that was in agreement with Hyer's analytical model. The in-plane strains and the out-of-plane displacement were approximated by quadratic polynomials containing only the terms with even power. Quadratic approximations are suitable for calculation of the stable shapes of a composite. However, features related to shape bifurcation such as snap-through loads [26] and geometric limits for bistability [27] cannot be accurately described using a second-order strain model. Cantera et al. [28] presented a modified approach to simulate snap-through loads involving a second order strain model that includes non-uniform curvatures and uniform through-thickness normal strain. Pirrera et al. [29] showed that shape bifurcation effects can be modeled accurately using seventh order polynomials for displacements in the strain model. With ninth order displacement polynomials or higher, one can simulate the intermediate stages of snap-through but at the expense of computational cost. Lamacchia et al. [30] presented a computationally efficient semi-analytical high-order model that features decoupled stretching and bending contributions via a semi-inverse formulation of the constitutive equations.

This paper presents a high-order analytical strain model to systematically explore the design space of bistable composites that have two sources of residual stress. The analysis is presented through the example of a mechanically-prestressed bistable composite. The stable shapes of a rectangular composite are simulated for limiting ratios of prestrain and side length to determine the domain of bistability. A case study comparing the composite's response to various actuation modes such as axial, transverse, and in-plane loading is presented. Tensile tests are conducted on fabricated composite samples and snap-through is recorded using a 3D motion capture system. The mechanical work associated with the measured force-deflection curves is compared with the simulated actuation work in the axial loading case. Finally, a sensitivity study is conducted to explain the effect of design parameters of the composite on its performance metrics, *viz.*, range of deformation, stiffness, and actuation energy.

2. Composite configuration

The composite consists of two anisotropic fiber-reinforced elastomeric strips that are laminated on either face of an isotropic core plate. The core is flexible but has a high in-plane (*XY*) modulus relative to a pure elastomer. The reinforced elastomers, also known as elastomeric matrix composites (EMC) [11], have unidirectional fibers oriented along the width (90° orientation) of the strip. The function of the fibers is to ensure zero in-plane Poisson's ratio [31,32]. The EMCs are fabricated by sandwiching two layers of unidirectional carbon fibers between a pair of pre-cured silicone rubber sheets (Fig. 2(a)-(d)). Prestress is applied to a 90° EMC by stretching it along its length and holding it between a pair of grips. Two 90° EMC strips are aligned in the composite in an orthogonal configuration. The EMCs are bonded in a sequence to a steel core while maintaining the composite in a flat shape (Fig. 2(e)-(f)). The design, construction, and functions of the composite are presented in detail in [10].

Prestrain in only one EMC results in a composite with a single stable cylindrical curvature (Fig. 3(a)) whereas prestrain in two EMCs yields

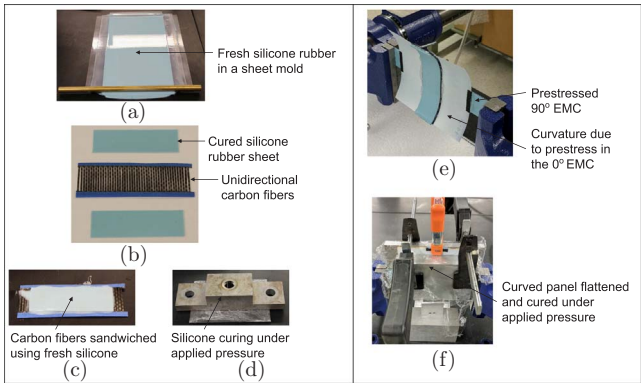

Fig. 2. Fabrication process for a mechanically-prestressed bistable laminate. Steps (a) through (d) pertain to EMC fabrication and steps (e) through (f) pertain to composite lamination.

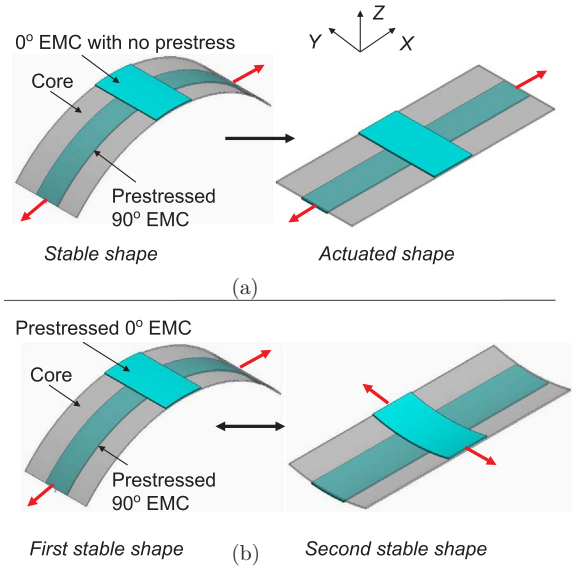

Fig. 3. Stable shapes of a mechanically-prestressed laminated composite.

two stable curvatures (Fig. 3(b)). When the prestressed EMCs are orthogonal to each other, the resulting stable shapes are said to be weakly coupled: each shape is influenced primarily by the EMC on the concave face. The prestressed EMC on the convex face has minimal effect on curvature due to its zero in-plane Poisson's ratio. The material properties and dimensions of each lamina influence both curvatures of the composite. EMC width is limited to a fraction of core width to minimize the restriction in deformation offered by the high-modulus fibers.

3. Analytical model

In this work, a mechanically-prestressed bistable composite is modeled as a laminated plate. The large out-of-plane deflection of the composite is described using a Lagrangian strain formulation in conjunction with classical laminate theory. Composite displacements are initially defined as unknown polynomial functions. The composite's strain energy is then computed and subsequently minimized to obtain a set of nonlinear equations that are a function of the coefficients of the displacement polynomials. These nonlinear equations are solved using the Rayleigh-Ritz method to calculate the shape of the composite. Cubic polynomials for displacement are sufficient to accurately calculate the stable shapes. However, an accurate description of the shape bifurcation phenomenon requires the use of higher order polynomials [29]. The iterative solution of nonlinear equations involving high-order displacement polynomials has been shown to be numerically ill-conditioned [33]. For purposes of numerical conditioning, composite displacements are presented in this study in non-dimensional form.

3.1. Non-dimensional composite displacements

The method for scaling used here was first presented by Stein [34]. It was implemented by Diaconu and Weaver [35] in the analysis of postbuckled orthotropic laminates, and by Pirrera et al. [29] in the high-order modeling of bistable laminates. The nondimensional displacements $(\tilde{u}_0,\tilde{v}_0,\tilde{w}_0)$ at an arbitrary point on the composite's geometric mid-plane are expressed in terms of its true displacements (u_0,v_0,w_0) in the (X,Y,Z) directions as:

$$\tilde{u}_0 = \frac{u_0}{U_0}, \quad \tilde{v}_0 = \frac{v_0}{V_0}, \quad \tilde{w}_0 = \frac{w_0}{W_0}, \tag{1}$$

where, U_0,V_0, and W_0 are scaling factors defined in terms of composite stiffness as:

$$U_0 = \frac{\sqrt{A_{11}^* A_{22}^* D_{11}^* D_{22}^*}}{L_x},$$
$$V_0 = U_0 \frac{L_x}{L_y},$$
$$W_0 = \sqrt{U_0 L_x}. \tag{2}$$

The terms A^* and D^* are defined as:

$$A^* = A^{-1}, \quad D^* = D - BA^{-1}B, \tag{3}$$

where A, B, and D are the extensional, coupled extension-bending, and bending stiffness matrices [36] of an n-layered composite expressed in terms of the plane-stress reduced stiffnesses $Q_{ij}\{i,j = 1,2,6\}$ as:

$$A_{ij} = \sum_{k=1}^{n} Q_{ij}^{(k)} (z_{k+1} - z_k),$$
$$B_{ij} = \frac{1}{2} \sum_{k=1}^{n} Q_{ij}^{(k)} (z_{k+1}^2 - z_k^2),$$
$$D_{ij} = \frac{1}{3} \sum_{k=1}^{n} Q_{ij}^{(k)} (z_{k+1}^3 - z_k^3). \tag{4}$$

The x and y coordinates are scaled as follows:

$$\tilde{x} = \frac{x}{L_x}, \quad \tilde{y} = \frac{y}{L_y}. \tag{5}$$

The ratio of EMC width to core width is defined as:

$$\alpha_0 = \frac{C_x}{L_x}, \quad \alpha_{90} = \frac{C_y}{L_y}. \tag{6}$$

3.2. Strain model

The composite's strains (Fig. 4), defined using a Lagrangian description as per Von Karman's hypothesis [37], are written in terms of non-dimensional displacements $(\tilde{u},\tilde{v},\tilde{w})$ as:

$$\epsilon_x = \frac{U_0}{L_x}\frac{\partial \tilde{u}}{\partial \tilde{x}} + \frac{1}{2}\frac{W_0^2}{L_x^2}\left(\frac{\partial \tilde{w}}{\partial \tilde{x}}\right)^2, \tag{7}$$

$$\gamma_{xy} = \frac{U_0}{L_y}\frac{\partial \tilde{u}}{\partial \tilde{y}} + \frac{V_0}{L_x}\frac{\partial \tilde{v}}{\partial \tilde{x}} + \frac{W_0^2}{L_x L_y}\frac{\partial \tilde{w}}{\partial \tilde{x}}\frac{\partial \tilde{w}}{\partial \tilde{y}}, \tag{8}$$

$$\epsilon_y = \frac{V_0}{L_y}\frac{\partial \tilde{v}}{\partial \tilde{y}} + \frac{1}{2}\frac{W_0^2}{L_y^2}\left(\frac{\partial \tilde{w}}{\partial \tilde{y}}\right)^2. \tag{9}$$

According to classical laminate theory, the composite's

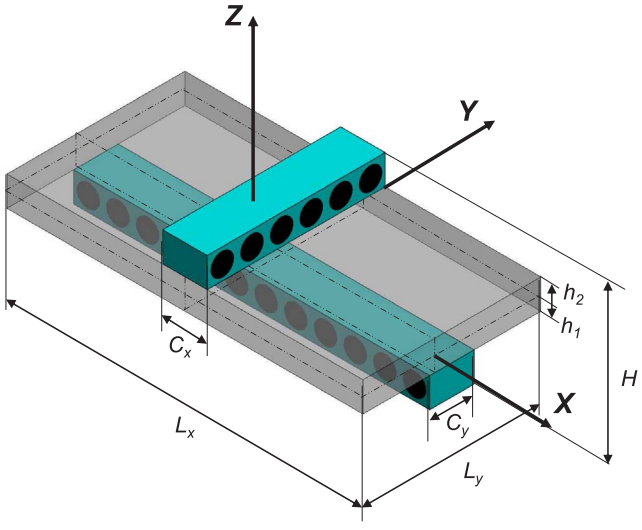

Fig. 4. Schematic representation of a mechanically-prestressed bistable laminate.

displacements can be written in terms of mid-plane displacements $(\tilde{u}_0,\tilde{v}_0,\tilde{w}_0)$ as:

$$\tilde{u}(\tilde{x},\tilde{y},z) = U_0\tilde{u}_0(\tilde{x}) - z\frac{W_0}{L_x}\frac{\partial\tilde{w}_0}{\partial\tilde{x}}, \tag{10}$$

$$\tilde{v}(\tilde{x},\tilde{y},z) = V_0\tilde{v}_0(\tilde{y}) - z\frac{W_0}{L_y}\frac{\partial\tilde{w}_0}{\partial\tilde{y}}, \tag{11}$$

$$\tilde{w}(\tilde{x},\tilde{y},z) = W_0\tilde{w}_0(\tilde{x},\tilde{y}). \tag{12}$$

Eqs. (10)–(12) are substituted into (7)–(9) to obtain the composite strains in terms of the displacements of the geometric mid-plane.

The displacements of the mid-plane, described using complete polynomials of order O_p, are of the form:

$$\tilde{u}_0 = \sum_{q=0}^{O_p}\sum_{p=0}^{q} b_{p,q-p}\tilde{x}^p\tilde{y}^{p-q}, \tag{13}$$

$$\tilde{v}_0 = \sum_{q=0}^{O_p}\sum_{p=0}^{q} c_{p,q-p}\tilde{x}^p\tilde{y}^{p-q}, \tag{14}$$

$$\tilde{w}_0 = \sum_{q=0}^{O_p}\sum_{p=0}^{q} d_{p,q-p}\tilde{x}^p\tilde{y}^{p-q}, \tag{15}$$

where O_p is the chosen order of the polynomial and $b_{p,q-p}$, $c_{p,q-p}$, and $d_{p,q-p}$ are coefficients that are to be evaluated.

3.3. Strain energy computation

The potential energy (Φ) of the composite is expressed in terms of the material and geometric properties of the laminae as:

$$\Phi = \int_V \left(\Phi_1 + Q_{12}\,\epsilon_x\epsilon_y + \Phi_2 + \frac{1}{2}Q_{16}\gamma_{xy}\,\epsilon_x + \frac{1}{2}Q_{26}\gamma_{xy}\,\epsilon_y + \frac{1}{2}Q_{66}\gamma_{xy}^2\right)dV. \tag{16}$$

The limits of integration are shown in Table 1. In this composite, the core is a linear isotropic material whereas the 90° and 0° EMCs are anisotropic materials with linear strains in all directions except x and y, respectively. For linearly strained directions, Φ_1 and Φ_2 are written per Hooke's law as $0.5(Q_{11}\,\epsilon_x^2)$ and $0.5(Q_{22}\,\epsilon_y^2)$, respectively. In the direction of prestrain, the constitutive law of an EMC is described using an experimentally-derived nonlinear expression [20] as:

$$\sigma = -0.698\,\epsilon^4 + 2.29\,\epsilon^3 - 2.306\,\epsilon^2 + 1.598\,\epsilon \quad [\text{MPa}]. \tag{17}$$

Strain energies Φ_1 and Φ_2 of the 90° and 0° EMCs respectively are computed as the integral of σ_x and σ_y based on (17). This gives:

$$\Phi_1^{(90)} = f(\epsilon_{90} - \epsilon_x), \quad \Phi_2^{(0)} = f(\epsilon_0 - \epsilon_y). \tag{18}$$

It is noted that strains ϵ_x,ϵ_y, and γ_{xy} are expressed in terms of scaled displacements and coordinates for purposes of numerical conditioning. On the other hand, prestrains ϵ_{90} and ϵ_0, applied to the EMCs prior to lamination, represent the input energy content and are hence not scaled.

3.4. Work done by external forces

Four cases of external forces acting on the composite are studied in this work (Fig. 5). The composite, shown in the YZ plane, is assumed to be clamped at its midpoint O and curved about the X axis in the unactuated state. Cases *1* to *3* represent actuation forces applied at points $A(0,-0.5)$ and $B(0,0.5)$ whereas case *4* represents a uniformly distributed operational load.

Table 1
Limits of integration for the computation of the total potential energy of a mechanically-prestressed bistable laminate.

Lamina	$\tilde{x}$	$\tilde{y}$	z
90° EMC	$(-1/2,1/2)$	$(-\alpha_{90}/2,\alpha_{90}/2)$	$(-H/2,-h_1)$
Core	$(-1/2,1/2)$	$(-1/2,1/2)$	$(-h_1,h_2)$
0° EMC	$(-\alpha_0/2,\alpha_0/2)$	$(-1/2,1/2)$	$(h_2,H/2)$

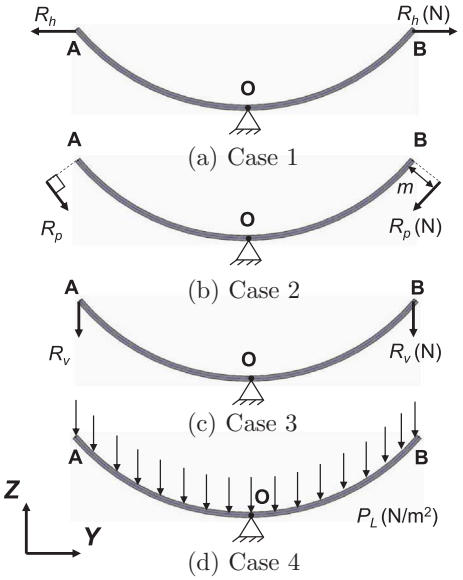

Fig. 5. Four cases for external forces applied on a bistable composite to effect snap-through into the second stable shape. The first three cases shown in (a) through (c) are point-wise forces whereas case four shown in (d) is a uniformly distributed force.

3.4.1. Case 1

The composite is actuated by applying a pair of equal and opposite forces $-R_h\hat{j}$ and $R_h\hat{j}$ at A and B, respectively (Fig. 5(a)). The variational work done by $\overrightarrow{R_h}$ is expressed as:

$$\delta W_h = -R_h V_0\tilde{v}_0|_{\{0,-0.5\}} + R_h V_0\tilde{v}_0|_{\{0,0.5\}}. \tag{19}$$

3.4.2. Case 2

In-plane actuation is represented by a pair of forces at A and B of magnitude R_p acting in a direction tangential to the geometric mid-plane (Fig. 5(b)). The force $\overrightarrow{R_p}$, located at an offset m from the mid-plane, is defined as:

$$\overrightarrow{R_{p(A)}} = \frac{R_p}{L_y}\frac{\partial\overrightarrow{r_p}}{\partial\tilde{y}}|_{\{0,-0.5\}}, \quad \overrightarrow{R_{p(B)}} = -\frac{R_p}{L_y}\frac{\partial\overrightarrow{r_p}}{\partial\tilde{y}}|_{\{0,0.5\}}. \tag{20}$$

The point of application of the force $\overrightarrow{r_p}$ is the sum of the position vector $(\overrightarrow{r})$ on the geometric mid-plane and the normal $(\overrightarrow{n})$ at $\overrightarrow{r}$

$$\overrightarrow{r_p} = \overrightarrow{r} + m.\,\overrightarrow{n}, \tag{21}$$

$$= ((L_x\tilde{x} + U_0\tilde{u}_0)\hat{i} + (L_y\tilde{y} + V_0\tilde{v}_0)\hat{j} + W_0\tilde{w}_0\hat{k}) + \frac{m}{L_xL_y}.\left(\frac{\partial\overrightarrow{r}}{\partial\tilde{x}} \times \frac{\partial\overrightarrow{r}}{\partial\tilde{y}}\right). \tag{22}$$

The variational work done by the pair of forces $\overrightarrow{R_p}$ (Fig. 5(c)) is written as:

$$\delta W_p = \overrightarrow{R_{p(A)}}.\,\delta\overrightarrow{r_p}|_{\{0,-0.5\}} + \overrightarrow{R_{p(B)}}.\,\delta\overrightarrow{r_p}|_{\{0,0.5\}}. \tag{23}$$

3.4.3. Case 3

The variational work done on a composite that is actuated by a transverse force $-R_v\hat{k}$ acting at A and B is written as:

$$\delta W_v = -R_v W_0\tilde{w}_0|_{\{0,-0.5\}} - R_v W_0\tilde{w}_0|_{\{0,0.5\}}. \tag{24}$$

3.4.4. Case 4

The operational load acting on a composite is represented as a uniformly distributed force (P_L) acting in the $-Z$ direction (Fig. 5(d)). The corresponding variational work is given by:

$$\delta W_l = \int_{-0.5}^{0.5}\int_{-0.5}^{0.5} P_L W_0 \widetilde{w}_0 \mathrm{d}x\mathrm{d}y. \tag{25}$$

The net variational work (δW) done on the composite by various actuation forces is written as:

$$\delta W = \delta W_p + \delta W_h + \delta W_v + \delta W_l. \tag{26}$$

3.5. Computation of composite shape

The equilibrium shapes of the composite are obtained as a function of actuation force by minimizing the net energy using the variational Rayleigh-Ritz approach:

$$\sum_i \frac{\partial(\Phi - W)}{\partial C_i} = 0, \tag{27}$$

where $C_i = \{b_{p,q-p}, c_{p,q-p}, d_{p,q-p}\}$ for p ranging from 0 to q and q ranging from 0 to O_p. The expressions for U_T, W, and their partial derivatives are derived in symbolic form using MAPLE. The nonlinear equations resulting from (27) are solved in MATLAB using the Newton-Raphson method. Composite shape is computed for various polynomial orders of the strain model. Prior to computation, the number of terms in the complete displacement polynomials is reduced by applying the conditions of symmetry. Since the composite is clamped at the center, $\widetilde{u}_0$ is odd in x and even in y,$\widetilde{v}_0$ is even in x and odd in y, and $\widetilde{w}_0$ is even in x and y and is zero at the center. The number of unknown coefficients for each polynomial order is shown in Table 2. The order of the strain energy integrand involving a mechanically-prestressed EMC is greater than twice that of the integrand for a thermally-cured FRP laminate with linear matrix material (Table 2); the order is directly proportional to the computational cost of the model. For polynomial orders 3–5, the computation was carried out on a standalone workstation whereas higher order polynomial models were simulated using clusters at the Ohio Supercomputer Center [38]. The computational cost can be lowered by 20% by reducing σ in (17) to a cubic function.

4. Experiments

Experimental measurement of the snap-through force of a bistable composite involves the application of a controlled force or displacement in a quasistatic setup. To this end, Dano and Hyer [39] applied a moment at two points on the composite in a three-point bending setup. They performed a force-controlled experiment where strain was measured using bonded strain gauges. Potter et al. [40] developed a position-controlled experiment to simultaneously measure the composite's displacement and the applied force. The sample was placed on its edges on a low-friction aluminum plate and a transverse point load was applied at the center using a steel ball. A perforated plate with holes in a

Table 2
Size of the displacement polynomials and strain energy integrand.

Order (n)	Reduced unknowns	Order of $\mathrm{d}\Phi(\widetilde{x},\widetilde{y})$	
		Prestressed EMC	Thermally-cured FRP
3	8	10	4
4	11	30	12
5	17	30	12
6	21	50	20
7	29	50	20
8	35	70	28
9	44	70	28

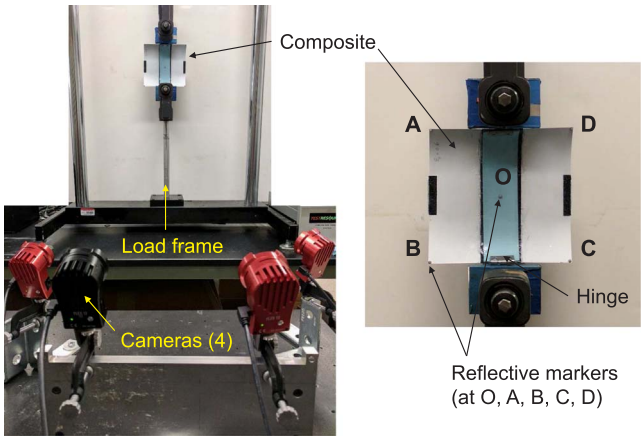

Fig. 6. Experimental setup to record shape transition in a bistable composite.

11 × 11 grid was aligned inline with the composite. Deformation at each position increment was measured through the holes with a caliper. Experiments revealed that the snap-through phenomenon comprises multiple events. In particular, one half of the composite undergoes a smooth shape transition leading to a partial snap-through, following which the other half snaps to the second stable shape. Cantera et al. [28] employed Potter's approach but used rods to suspend the composite at its vertices for reduced friction. Tawfik et al. [41] presented an improved frictionless experimental setup in which the edges of the composite slide on an air cushion.

The proposed experimental procedure involves a uniaxial tensile test in which a curved composite is deformed until snap-through occurs (Fig. 6). Given that the composite's shapes are weakly coupled, it is sufficient to record actuation from the first shape to the second. The straight edges *AD* and *BC* of a cylindrical composite are held in the load frame at their midpoint using small hinges. The hinges are bonded to the EMC on the concave side and their axis of rotation are parallel to the respective straight edges. There is no sliding or rolling contact with the composite. The head of the load frame (Test Resources Inc.) moves vertically and measures the force profile using an inline 200 N load cell. The displacement of the frame head is recorded by a rotary encoder. Tip displacement is separately measured by a 3D motion capture system; the frame measures displacement only up to snap-through. Betts et al. [42] used a video camera system that tracks circular markers to measure the stable shapes of a bistable laminate. In the present setup, hemispherical reflective markers of 3 mm diameter are placed at the center (O) and the four vertices (A, B, C, D) of a square laminate. A set of four still cameras (OptiTrack, Natural Point Inc.), with a resolution of 1.3 megapixels, is used to record the position of each marker through coordinate triangulation. The cameras are mounted to have a capture volume of 1.1 × 1.1 × 1.1 (m).

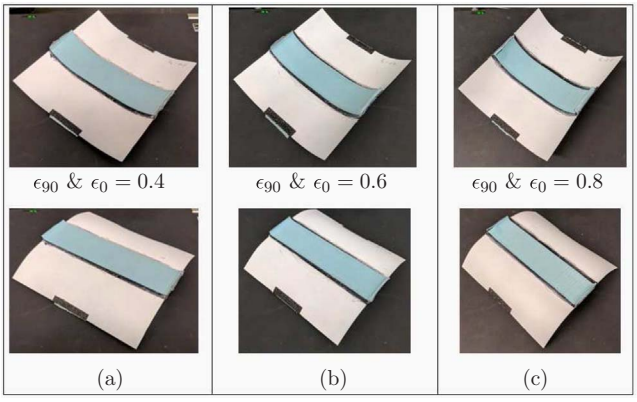

Fig. 7. Fabricated samples of a mechanically-prestressed bistable laminate.

Table 3
Laminae dimensions of a bistable composite for modeling and experiments.

Lamina	Length (mm)	Width (mm)	Thickness (mm)
90° EMC	152.4	38.1	2.032
Core	152.4	152.4	0.127
0° EMC	38.1	152.4	2.032

Square test samples are fabricated in the 90° EMC/core/0° EMC configurations with equal prestrain values of 0.4, 0.6, and 0.8 in both EMCs (Fig. 7). The dimensions of the laminae are shown in Table 3. Prior to testing, the cameras are calibrated to an accuracy of 0.021 mm by waving a calibration wand that contains inline markers over a span of 250 mm. The coordinate system is defined using markers mounted on the ends of a right angle measure. To simplify data processing, the axes (X,Y,Z) are defined such that the XY plane is aligned parallel to the plane containing the composite's vertices (markers). Quasistatic tensile tests are conducted on each sample by moving the frame head at a rate of 5 mm/min until the composite snaps into its second shape. The load frame and the motion capture system are synchronized to record displacement at 10 frames per second. Each sample is tested five times for repeatability. Measurements from the fifth test are presented in this paper.

The out-of-plane tip deflection w_0 is calculated for each straight edge $(\overline{AD},\overline{BC})$ as the average of the z displacements of its vertices. The respective deflections w_{AD} and w_{BC} of $\overline{AD}$ and $\overline{BC}$ evolve differently with time and actuation force as shown in Fig. 8. At $w_{AD} = 0$, $w_{BC} > w_{AD}$ and w_{AD} is continuous (Fig. 8(a)). In the vicinity of $w_{BC} = 0$, both w_{AD} and w_{BC} are discontinuous (Fig. 8(b)). The sharp drop in displacement at the discontinuity occurs in two stages. The drop in force in the first stage is partial, indicating an intermediate shape in the snap-through event (Fig. 8(b)). Snapshots of the shape transition are shown in Fig. 9. Upon flattening, the composite snaps partially into an intermediate stable shape that has $\overline{AD}$ in its second curved shape while $\overline{BC}$ remains straight (Fig. 9(b)). Flattening the composite further results in a full-snap through in which $\overline{BC}$ snaps into the second curved shape and both edges reach equilibrium simultaneously (Fig. 9(c)). The snap-through behavior of the tested samples is similar to that of the thermally-cured FRP laminates tested by Potter et al. [40].

5. Results and discussion

Results based on experiments and model-based simulations are presented in the following sequence:

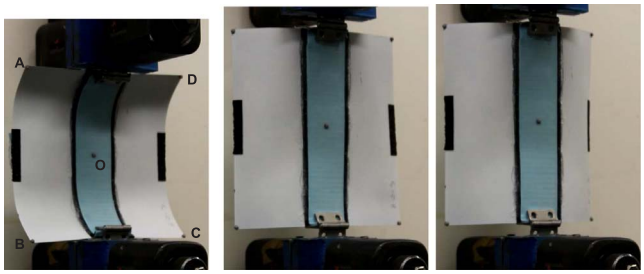

(a) $t = 0$ s (b) $t = 367$ s (c) $t = 373$ s

Fig. 9. Composite shape with $\epsilon_0 = \epsilon_{90} = 0.8$ in (a) unactuated first stable state, (b) intermediate stable state during snap-through, and (c) second stable state post snap-through.

- The stable shapes of a square laminate are calculated as a function of ϵ_{90} and ϵ_0 for various orders of the displacement polynomials. Subsequent results are presented using a chosen high-order polynomial.
- The effect of aspect ratio on the bistability regime of rectangular laminates is simulated as a function of ϵ_{90} and ϵ_0.
- Work done on a square composite is computed for force cases 1 to 3. The analytical model is validated against measured data.
- The sensitivity of the composite's tip displacement (w_0), stiffness to transverse pressure (K_L), and snap-through work (W_p) done by an in-plane actuator, are analyzed for a given change in core modulus and thickness.

Simulations conducted using the analytical model presented in Section 2 yield two stable cylindrical shapes in the unactuated state. The dimensions and measured material properties of the laminae used for both simulation and experiments are shown in Tables 3 and 4, respectively. The longitudinal modulus (E_1) of a 90° EMC strip is a nonlinear function of strain and its constitutive response is measured through a uniaxial tensile test (see (17)). For the calculation of the scaling factors U_0, V_0, and W_0, E_1 of a 90° EMC is averaged to be 1.5 MPa over a strain range of 0 to 1. The transverse EMC modulus (E_2), assumed to be 0.4 MPa, corresponds to shear in a pure elastomer; the core and the fiber-reinforced elastomeric layer in the EMC are separated by a purely-elastomeric sub layer [10]. The in-plane shear modulus (G_{12}) for both EMCs is assumed to be 0.8 times E_1 [31]. In the following analyses, the composite is considered to be initially curved about the X axis.

The composite's tip displacement (w_0) in the unactuated state is calculated as a function of prestrain ratio ϵ_r ($= \epsilon_0/\epsilon_{90}$) ranging from 0.01 to 1 while ϵ_{90} is maintained constant at 1. Fig. 10 shows w_0 as a

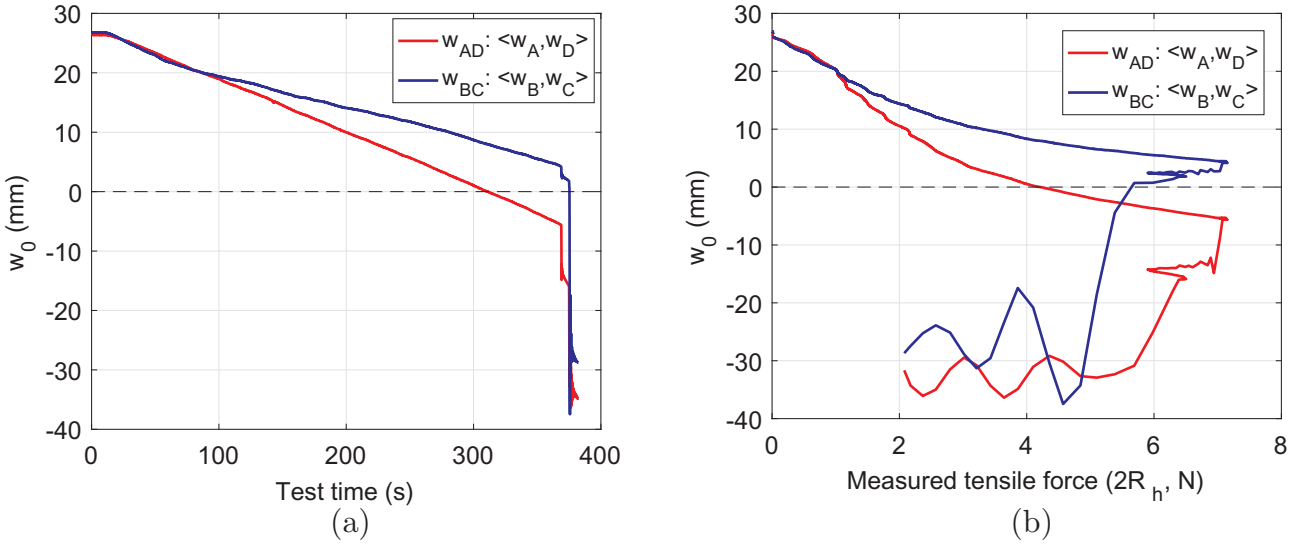

Fig. 8. Measured out-of-plane displacements of $\overline{AD}$ and $\overline{BC}$, as a function of (a) time and (b) actuation force, in a composite with $\epsilon_0 = \epsilon_{90} = 0.8$.

Table 4
Material properties of the laminae of modeled and tested prestressed composites.

Lamina	E_1 (MPa)	E_2 (MPa)	G_{12} (MPa)	ν_{12}	ν_{21}
90° EMC	Nonlinear	0.4	1.2	0	0
Core layer	200,000	200,000	78,125	0.28	0.28
0° EMC	0.4	Nonlinear	1.2	0	0

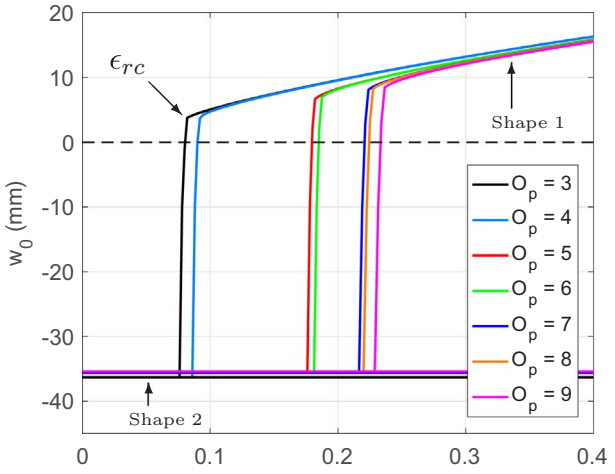

Fig. 10. Composite shapes as a function of prestrain ratio ϵ_r for $\epsilon_{90} = 1$.

function of ϵ_r for various orders of the displacement polynomials; the first half of ϵ_r is emphasized to illustrate the loss in bistability at its lower extremity. Displacement w_0, corresponding to the first shape, decreases with a decrease in ϵ_r until a critical ratio ϵ_{rc} where the shape ceases to exist. Below ϵ_{rc}, the composite is stable only in the second cylindrical shape. Shape 2, as indicated in Fig. 10, is influenced by ϵ_{90} and is invariant to changes in ϵ_0 when $\epsilon_r < 1$. Since the stable shapes are weakly coupled, similar results are obtained at the higher extremity of ϵ_r; the same analysis with ϵ_{90} ranging from 0 to 1 at $\epsilon_0 = 1$ yields the higher extremity. Such an envelope for bistability is characteristic of laminates that have two sources of prestress. Thermally cured FRP laminates have a single source of residual stress and exhibit a saddle shape (small deformation) outside the domain of bistability.

With an increase in polynomial order from three to nine, ϵ_{rc} increases to converge to a particular value. Further, the displacement w_0 at ϵ_{rc} is higher in higher-order models. For $\epsilon_r > \epsilon_{rc}$, the difference in w_0 among various polynomial orders is negligible. ϵ_{rc} for each polynomial of type O_{2p} ($p > 2$) is close to that of the odd-order polynomial of type O_{2p-1}. Due to the imposed symmetry conditions on $\widetilde{u}_0$,$\widetilde{v}_0$, and $\widetilde{w}_0$, the additional terms in O_{2p} relative to O_{2p-1} are seen only in $\widetilde{w}_0$. Therefore, out-of-plane deflection w_0 has a minor effect on ϵ_{rc} whereas in-plane strain has a dominant effect. In the third, seventh, and ninth order cases, ϵ_{rc} is 0.082, 0.224, and 0.236 respectively. Given the marginal increase in model accuracy from seventh to ninth order, seventh order displacement polynomials are chosen for further analysis in the interest of computational cost (see Table 2).

The effect of aspect ratio AR (L_y/L_x) is simulated at $L_x = 152.4$ mm by varying one EMC prestrain at a time. In the first case, a constant prestrain $\epsilon_{90} = 0.6$ is maintained in the EMC on the convex face (Fig. 11(a)). The value of AR corresponding to the loss of bistability increases with an increase in ϵ_0. Beyond the critical value of AR, only one stable cylindrical shape exists (as in Fig. 3(a)). When ϵ_0 is treated to be constant (at 0.6), the limiting AR increases with an increase in ϵ_{90} (Fig. 11(b)). An increase in aspect ratio for a given width is associated with an increase in the strain energy of the core, thereby requiring higher prestrains with ϵ_r close to 1 for the existence of bistability.

Work done on the composite by external forces in cases one to three (Fig. 5) is computed as per (19), (23), and (24). For comparison, W_h, W_p, and W_v are plotted as a function of tip displacement w_0.

The simulated actuation work W_h is compared with the corresponding experimentally measured values to validate the analytical model (Fig. 12). Flattening of the composite is associated with an exponential increase in W_h up to the point of snap-through. Post snap-through, experiments indicate a small drop in W_h followed by a sharper drop before reaching a steady value as w_0 tends to zero. The existence of two energy peaks is consistent with the observation (Section 4) that in the chosen laminate configuration, snap-through occurs in two stages. Energy peaks are not seen in the simulated curves because displacements are calculated as a function of a monotonically increasing force R_h; at snap-through, there is a sharp drop in w_0 but not R_h. For all practical purposes, snap-through force and tip displacement profile are sufficient to design actuators for bistable composites. The simulated energy profile is in agreement with experimental data. The model overpredicts snap-through energy by 7.7%, 12.1%, and 6.7% with respect to the measured value (higher peak) in samples with prestrains of 0.4, 0.6, and 0.8, respectively. The corresponding error in the simulated tip displacement at snap-through relative to the measured displacement (at higher peak) is 6.2%, 2.43%, and −8.8%. Higher model accuracy can be achieved by increasing the order of the displacement polynomials.

Fig. 13(a) shows the energy profile pertaining to an in-plane force R_p applied at the geometric mid-plane ($m = 0$); prestrains ϵ_0 and ϵ_{90} are assumed to be equal. The energy required for snap-through increases with an increase in ϵ_0. Further, snap-through is initiated at a higher displacement w_0 for higher values of ϵ_{90}. Fig. 13(b) shows the energy profile for non-zero values of the force offset m from the geometric mid-plane at constant values of ϵ_0 and ϵ_{90} of 0.6. Increasing the offset towards the convex face of the composite ($m > 0$) results in a decrease in snap-through energy. This behavior is attributed to the associated reduction in the total displacement recovered by a given R_p (see (10)–(12)). Moving the actuator towards the concave face results in an exponential increase in snap-through energy.

The actuation energy associated with a transverse force is simulated for various values of ϵ_0 assuming ϵ_0 and ϵ_{90} are equal (Fig. 14). While W_v has a similar trend as W_h and W_p, it is worth noting that force R_v varies linearly with w_0 whereas R_h and R_v vary exponentially (not illustrated). A comparison of the various energy profiles of actuation forces acting at points A and B (Fig. 5) shows that for a given actuation stroke, W_h is an order of magnitude higher than W_v and W_p is an order of magnitude higher than W_h. Therefore, the minimum and maximum energy configurations are associated with a pure moment and a pure in-plane force respectively. Also, the displacement w_0 at which snap-through occurs is highest in the case of a moment and least when actuated by an in-plane force.

6. Sensitivity study

The parameters that quantify the composite's morphing performance are: displacement w_0 in the unactuated state; stiffness K_L to transversely-applied pressure P_L (case 4); and work W_p done by an in-plane force R_p to achieve snap-through from a stable initial shape. Fig. 15(a) shows the effect of core modulus ranging from 100 to 200 GPa on the composite's performance parameters; thickness is maintained constant at 0.127 mm. Each parameter is normalized with respect to the lowest value in the simulated range. Increasing the modulus by 100 GPa yields a reduction in w_0 by 48.3%. On the other hand, K_L, and W_p increase by 93.3%, and 18.1% respectively. Sensitivity of the parameters to core thickness is shown in Fig. 15(b); core modulus is assumed to be 100 GPa. Doubling the core's thickness results in −83.8%, 520%, and −10.5% change in w_0,K_L, and W_p respectively.

An increase in core modulus or thickness translates to an increase in strain energy and hence a decrease in out-of-plane deformation for a given prestress configuration; deformation is more sensitive to thickness change. A decrease in deformation is accompanied by an increase in

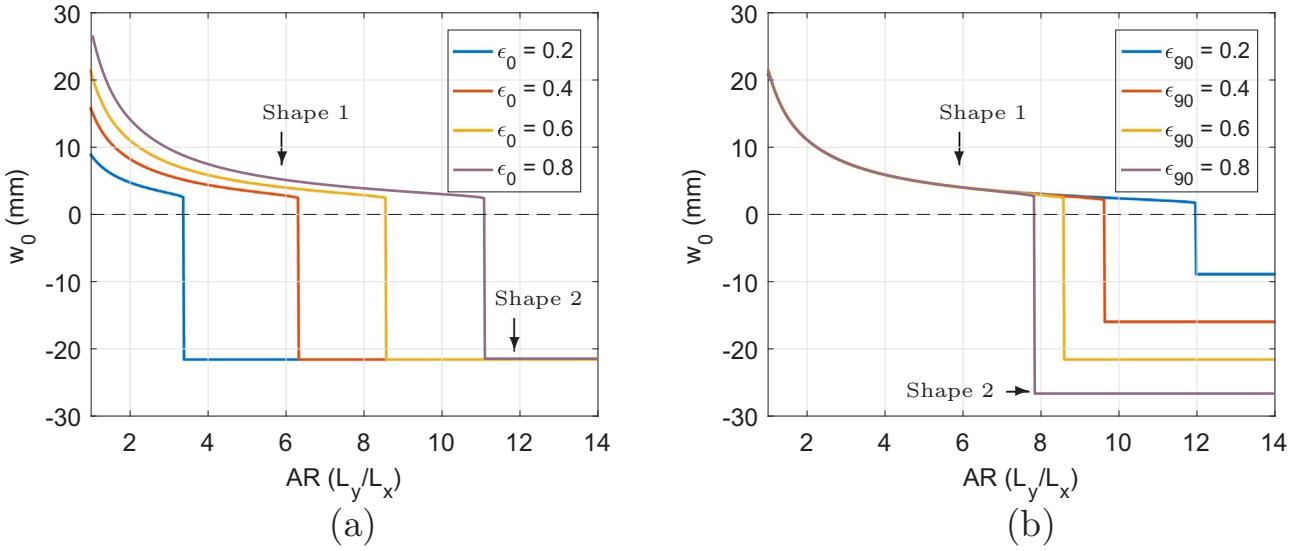

Fig. 11. Effect of aspect ratio *AR* on the composite's stable shapes as a function of (a) ϵ_0 while $\epsilon_{90} = 0.6$ and (b) ϵ_{90} while $\epsilon_0 = 0.6$.

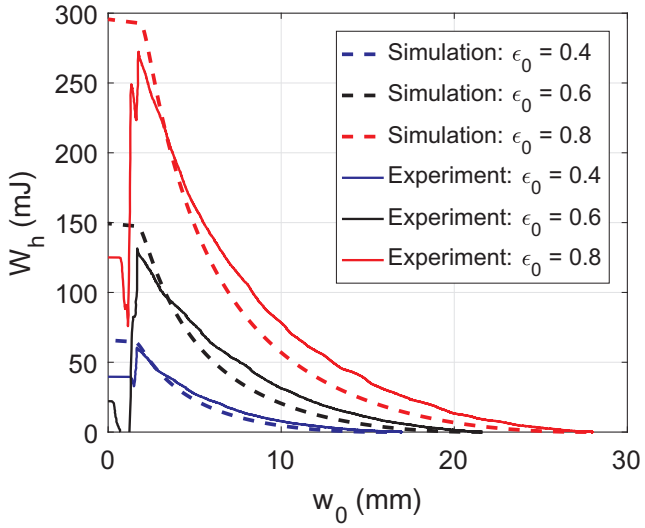

Fig. 12. Work done by an axial force R_h on a composite with $\epsilon_{90} = \epsilon_0$.

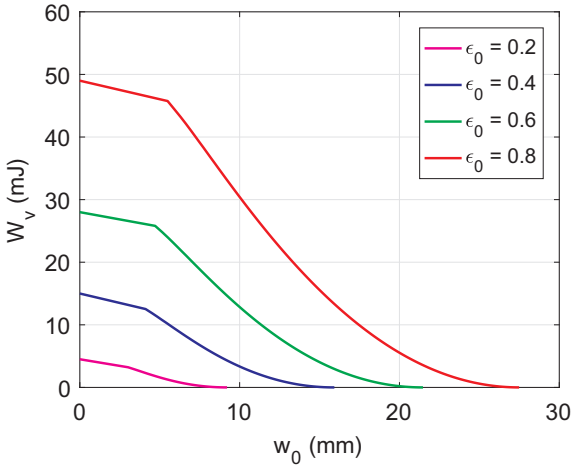

Fig. 14. Work done by a transverse force R_v as function of ϵ_0 where $\epsilon_{90} = \epsilon_0$.

stiffness for any modulus or thickness. Stiffness is more sensitive to thickness than to modulus due to the cubic dependence of the stiffness matrix coefficients on thickness in (4). Higher actuation work is required to recover the strain energy associated with higher core modulus. Among the three performance parameters, stiffness is the most sensitive to the core's properties whereas actuation energy is the least.

7. Concluding remarks

The limits of bistability of rectangular laminates with two sources of prestress are studied for the first time through this work. A novel experimental procedure, involving friction-free tensile testing and 3D motion capture, is presented to study the snap-through characteristics of mechanically-prestressed composites. Experiments show that these composites exhibit a multi-stage snap-through phenomenon akin to that

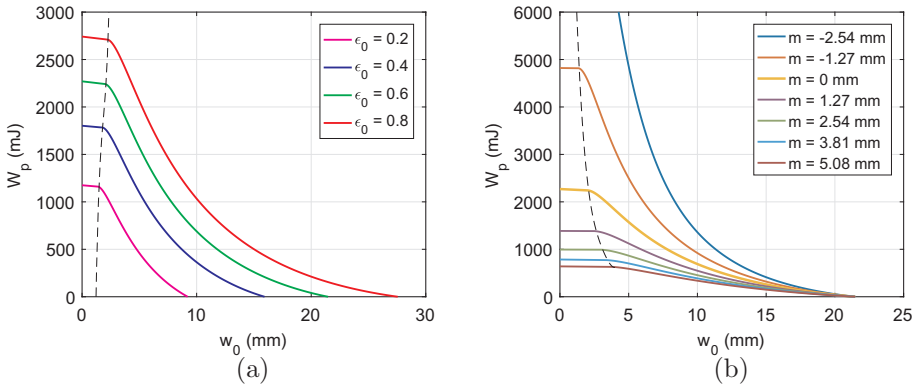

Fig. 13. Work done by an in-plane actuation force R_p as a function of (a) ϵ_0 where $m = 0$ and $\epsilon_{90} = \epsilon_0$, and (b) m where $\epsilon_0 = \epsilon_{90} = 0.6$.

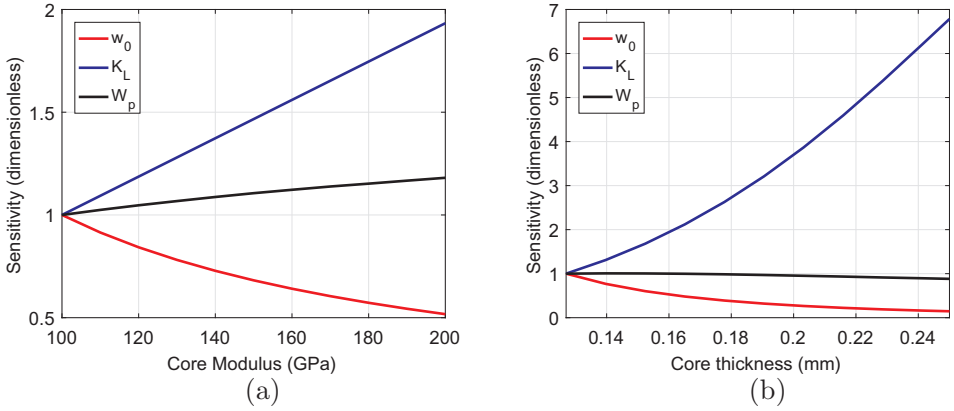

Fig. 15. Sensitivity of the composite's performance to (a) core modulus and (b) core thickness.

seen in thermally-cured FRP laminates. A high-order strain model is developed to accurately determine the composite's domain of bistability as a function of prestrain ratio. The aspect ratio limit for bistability can be extended by increasing prestrain in both EMCs and by maintaining the prestrain ratio close to one. A distinct feature in orthogonal-ply bistable composites with two sources of mechanical prestress is that they need not be symmetric along the thickness. Further, loss in bistability due to insufficient prestress in one EMC yields a single cylindrical shape. A comparison of various actuation modes using the experimentally-validated analytical model shows that the application of a moment requires the least amount of energy. In-plane actuation, which is made practically viable by smart materials, is relatively energy efficient when the actuator is mounted on the convex face of a curved composite. Among the evaluated performance parameters, out-of-plane stiffness and actuation (in-plane) energy are respectively found to be the most and least sensitive to the core's properties. Mechanically-prestressed composites offer possibilites for the design of active bistable elements for morphing panels.

Acknowledgments

Financial support was provided by the member organizations of the Smart Vehicle Concepts Center, a National Science Foundation Industry-University Cooperative Research Center (www.SmartVehicleCenter.org). Additional support for S.C. was provided by a Smart Vehicle Center Graduate Fellowship. Technical advice was provided by Dr. Umesh Gandhi and Mr. Kazuhiko Mochida from Toyota Technical Center (TEMA-TTC) in Ann Arbor, MI.

References

[1] Bowman J, Sanders B, Weisshaar T. Evaluating the impact of morphing technologies on aircraft performance. In: 43rd AIAA/ASME/ASCE/AHS/ASC structures, structural dynamics, and materials conference, 22–25 Apr., Denver, CO; 2002. p. 1631.
[2] Barbarino S, Bilgen O, Ajaj RM, Friswell MI, Inman DJ. A review of morphing aircraft. J Intell Mater Syst Struct 2011;22(9):823–77.
[3] Daynes S, Weaver PM. Review of shape-morphing automobile structures: concepts and outlook. Proc Inst Mech Eng Part D: J Automobile Eng 2013;227(11):1603–22.
[4] Hyer MW. Some observations on the cured shape of thin unsymmetric laminates. J Compos Mater 1981;15(2):175–94.
[5] Daynes S, Diaconu CG, Potter KD, Weaver PM. Bistable prestressed symmetric laminates. J Compos Mater 2010;44(9):1119–37.
[6] Daynes S, Potter KD, Weaver PM. Bistable prestressed buckled laminates. Compos Sci Technol 2008;68(15–16):3431–7.
[7] Li H, Dai F, Weaver PM, Du S. Bistable hybrid symmetric laminates. Compos Struct 2014;116:782–92.
[8] Daynes S, Weaver P. Analysis of unsymmetric CFRP–metal hybrid laminates for use in adaptive structures. Compos Part A: Appl Sci Manuf 2010;41(11):1712–8.
[9] Chillara VSC, Headings LM, Dapino MJ. Self-folding laminated composites for smart origami structures. In: ASME 2015 conference on smart materials, adaptive structures and intelligent systems, 21–23 Sep., Colorado Springs, CO; 2015. p. 8968.
[10] Chillara VSC, Dapino MJ. Mechanically-prestressed bistable composite laminates with weakly coupled equilibrium shapes. Compos Part B: Eng 2017;111:251–60.
[11] Bubert EA, Woods BKS, Lee K, Kothera CS, Wereley NM. Design and fabrication of a passive 1D morphing aircraft skin. J Intell Mater Syst Struct 2010;21(17):1699–717.
[12] Lachenal X, Daynes S, Weaver PM. A zero torsional stiffness twist morphing blade as a wind turbine load alleviation device. Smart Mater Struct 2013;22(6):065016.
[13] Schultz MR. A concept for airfoil-like active bistable twisting structures. J Intell Mater Syst Struct 2008;19(2):157–69.
[14] Lee AJ, Moosavian A, Inman DJ. A piezoelectrically generated bistable laminate for morphing. Mater Lett 2017;190:123–6.
[15] Lacasse S, Terriault P, Simoneau C, Brailovski V. Design, manufacturing, and testing of an adaptive composite panel with embedded shape memory alloy actuators. J Intell Mater Syst Struct 2014;26(15):2055–72.
[16] Dano ML, Hyer MW. SMA-induced snap-through of unsymmetric fiber-reinforced composite laminates. Int J Solids Struct 2003;40(22):5949–72.
[17] Hufenbach W, Gude M, Czulak A. Actor-initiated snap-through of unsymmetric composites with multiple deformation states. J Mater Process Technol 2006;175(1–3):225–30.
[18] Chillara VSC, Dapino MJ. Bistable morphing composites with selectively-prestressed laminae. In: SPIE 2017 conference on smart structures and non-destructive evaluation, 25 Mar., Portland, OR; 2017. p. 10165–28.
[19] Feng N, Liu L, Liu Y, Leng J. A bio-inspired, active morphing skin for camber morphing structures. Smart Mater Struct 2015;24(3):035023.
[20] Chillara VSC, Headings LM, Dapino MJ. Multifunctional composites with intrinsic pressure actuation and prestress for morphing structures. Compos Struct 2016;157:265–74.
[21] Hyer MW. The room-temperature shapes of four-layer unsymmetric cross-ply laminates. J Compos Mater 1982;16(4):318–40.
[22] Hamamoto A, Hyer MW. Non-linear temperature-curvature relationships for unsymmetric graphite-epoxy laminates. Int J Solids Struct 1987;23(7):919–35.
[23] Dano ML, Hyer MW. The response of unsymmetric laminates to simple applied forces. Mech Compos Mater Struct 1996;3(1):65–80.
[24] Dano ML, Hyer MW. Thermally-induced deformation behavior of unsymmetric laminates. Int J Solids Struct 1998;35(17):2101–20.
[25] Schlecht M, Schulte K. Advanced calculation of the room-temperature shapes of unsymmetric laminates. J Compos Mater 1999;33(16):1472–90.
[26] Diaconu CG, Weaver PM, Arrieta AF. Dynamic analysis of bi-stable composite plates. J Sound Vibr 2009;322(4–5):987–1004.
[27] Gigliotti M, Wisnom MR, Potter KD. Loss of bifurcation and multiple shapes of thin [0/90] unsymmetric composite plates subject to thermal stress. Compos Sci Technol 2004;64(1):109–28.
[28] Cantera MA, Romera JM, Adarraga I, Mujika F. Modelling of [0/90] laminates subject to thermal effects considering mechanical curvature and through-the-thickness strain. Compos Struct 2014;110:77–87.
[29] Pirrera A, Avitabile D, Weaver PM. Bistable plates for morphing structures: a refined analytical approach with high-order polynomials. Int J Solids Struct 2010;47(25–26):3412–25.
[30] Lamacchia E, Pirrera A, Chenchiah IV, Weaver PM. Morphing shell structures: a generalised modelling approach. Compos Struct 2015;131:1017–27.
[31] Murray G, Gandhi F, Bakis C. Flexible matrix composite skins for one-dimensional wing morphing. J Intell Mater Syst Struct 2010;21(17):1771–81.
[32] Murugan S, Saavedra Flores EI, Adhikari S, Friswell MI. Optimal design of variable fiber spacing composites for morphing aircraft skins. Compos Struct 2012;94(5):1626–33.
[33] Wall WA, Gee M, Ramm E. The challenge of a three-dimensional shell formulation-the conditioning problem. In: Proceedings of ECCM, Athens, Greece; 2000. p. 99.
[34] Stein M. Postbuckling of orthotropic composite plates loaded in compression. Am Inst Aeronaut Astronaut J 1983;21(12):1729–35.
[35] Diaconu CG, Weaver PM. Postbuckling of long unsymmetrically laminated composite plates under axial compression. Internat J Solids Struct 2006;43(22–23):6978–97.
[36] Hyer MW. Stress analysis of fiber-reinforced composite materials. DEStech Publications, Inc; 2009.
[37] Reddy JN. Mechanics of laminated composite plates – theory and analysis. Boca Raton, FL: CRC Press; 1997.
[38] Center OS. Ohio supercomputer center; 1987. http://osc.edu/ark:/19495/f5s1ph73.
[39] Dano ML, Hyer MW. Snap-through of unsymmetric fiber-reinforced composite laminates. Int J Solids Struct 2002;39(1):175–98.
[40] Potter K, Weaver P, Seman AA, Shah S. Phenomena in the bifurcation of unsymmetric composite plates. Compos Part A: Appl Sci Manuf 2007;38(1):100–6.
[41] Tawfik SA, Stefan Dancila D, Armanios E. Planform effects upon the bistable response of cross-ply composite shells. Compos Part A: Appl Sci Manuf 2011;42(7):825–33.
[42] Betts DN, Salo AIT, Bowen CR, Kim HA. Characterisation and modelling of the cured shapes of arbitrary layup bistable composite laminates. Compos Struct 2010;92(7):1694–700.